arXiv:1401.4376v2 [cond-mat.mtrl-sci] 25 Mar 2014

Importance of relativistic effects in electronic structure and thermopower calculations for Mg_2Si, Mg_2Ge and Mg_2Sn.

K. Kutorasinski,* B. Wiendlocha, J. Tobola, and S. Kaprzyk
AGH University of Science and Technology,
Faculty of Physics and Applied Computer Science,
Al. A. Mickiewicza 30, 30-059 Krakow, Poland

(Dated: February 27, 2022)

We present a theoretical study of the influence of the relativistic effects on electronic band structure and thermopower of Mg_2X (X = Si, Ge, Sn) semiconductors. The full potential Korringa-Kohn-Rostoker (KKR) method is used, and the detailed comparison between the fully relativistic and semi-relativistic electronic structure features is done. We show that the spin-orbit (S-O) interaction splits the valence band structure at Γ point in good agreement with the experimental data, and this effect strongly depends on X atom. The S-O modifications of the topology of the Γ−centered hole-like Fermi surface pockets lead to a change in electron transport properties, which are investigated using the Boltzmann approach. In addition, the simple and efficient method is presented for the calculation of density of states effective mass m^*, and then used to examine the impact of relativistic effects on m^*. It is found that S-O coupling of the valence bands reduces effective mass and therefore significantly lowers the thermopower, primarily in Mg_2Sn, but also in Mg_2Ge. A detrimental influence of the S-O interaction on thermoelectric performance of $p-$type Mg_2X is analyzed in function of temperature ($10 - 900$ K) and carrier concentration ($10^{18} - 10^{22}$ cm^{-3}). Interestingly, similar calculations in $n-$type Mg_2X, show negligible effect of the S-O interaction on lowest conduction bands and consequently also on the Seebeck coefficient.

I. INTRODUCTION

The well-known Mg_2X (X = Si, Ge, Sn) thermoelectric compounds[1,2] and their alloys[3–5] have attracted renewed attention[6,7] as they are composed of abundant, low-cost (except germanium) and relatively non-toxic elements. These compounds exhibit large Seebeck coefficient (S), quite high electrical conductivity (σ) and low thermal conductivity (κ), yielding high efficiency of thermoelectric (TE) conversion, which is commonly captured in the dimensionless figure of merit $zT = \frac{\sigma S^2}{\kappa} T$ (T is the absolute temperature). The fact that some of these materials have $zT > 1$ in the mid-temperature range (400-800 K) and the lowest density amongst all efficient thermoelectrics[8], may prove to be decisive for ground transportation and space applications of these materials[9].

In particular, $n-$type $Mg_2Si_{1-x}Sn_x$ solid solutions have been found to be the most favorable in terms of TE energy conversion as they have the lowest thermal conductivity due to the maximum mass difference between its components and quite large effective mass of carriers[6]. It was reported that more complex quasi-quaternary solid solutions $Mg_2Si_{1-x-y}Sn_xGe_y$ exhibited even better TE performance upon $n-$type doping ($zT \sim 1.4$)[10]. Conversely, $p-$type Mg_2Si-based materials show markedly poorer TE performance ($zT < 0.4$) and there are only few impurities (Ga[11] or Ag[7,12]) which allow to turn these systems to the hole-like electrical conductivity and positive thermopower.

In order to elucidate unusual electron transport properties of Mg_2(Si-Ge-Sn) thermoelectrics, *ab initio* electronic structure calculations have been recently reported[13–16]. They mostly focused on so-called convergence of two conduction bands[13,16,17], which appeared near X point in the Brillouin zone of $Mg_2Si_{1-x}Sn_x$ for $x \sim 0.7$. Indeed, this electronic structure feature, expected to be responsible for overall enhancement of TE properties of these compounds, was supported by computations of relevant transport coefficients within the Boltzmann transport theory[14,16], but neglecting relativistic effects. We will show that the S-O interaction is crucial to reliably interpret especially $p-$type materials. Other theoretical works attempted to search for efficient $n-$ and $p-$ dopants to allow tuning and optimizing TE properties of these materials[9,18].

This work presents results of the first principles calculations performed by fully relativistic and semi relativistic Korringa-Kohn-Rostoker (KKR) methods combined with the Boltzmann transport approach to calculate thermopower in function of temperature and carrier concentration. We show that the S-O interaction strongly affects top valence bands near Γ point (best seen in Mg_2Sn) and the calculated values of the S-O splitting remain in good agreement with available experimental data. On the whole, the S-O coupling has a detrimental effect on $p-$type thermopower even at elevated temperature (300-400 K) and near optimal carrier concentration ($\sim 10^{20}$ cm^{-3}). On the other hand, the influence of the S-O coupling on conduction bands in $n-$type Mg_2X is negligible whatever temperature and carrier concentration.

The paper is organized as follows. Key formulas connecting the electronic band structure obtained from Korringa-Kohn-Rostoker (KKR) method and the electron transport coefficients studied within the Boltzmann approach, as well as computational details are given in Sec. II. Sec. III presents our results containing mainly (i) an analysis of the hole-like and electron-like Fermi surface shapes, (ii) a determination of effective mass of carriers

using a simple and efficient procedure, (iii) a discussion of Seebeck coefficient vs. temperature and concentration. All results derived from semi-relativistic and fully relativistic KKR calculations are compared in systematic way. The paper is concluded in Sec. IV.

II. THEORETICAL DETAILS

A. KKR band structure

The full potential KKR[19–24] method based on the Green's function multiple scattering theory was implemented to calculate electronic band structure. The reduction of the Dirac equation to the so-called semi-relativistic (SR) version was done with adopting technique developed by Koelling and Harmon[25] and extended by Ebert[26]. With this procedure the resulting set of coupled radial equation after dropping the spin-orbit interaction are similar to the non-relativistic one, but retains all other kinematic effects such as mass-velocity, Darwin contribution and higher order terms. The full relativistic (FR) method was done by directly solving the four component Dirac equation without any simplification. This allows to calculate band structure with or without S-O interaction, showing its influence directly. Electronic structure calculations were performed with previously presented details[23,27].

As already discussed in literature[14,31], LDA (and GGA as well) tends to underestimate band gaps also in Mg_2X compounds. In recent works[9,14] it was shown that the application of the modified Becke-Johnson semi-local exchange potential of Tran and Blaha[31] yielded the gap values close to the experimental ones but without important changes in shape of bands. Thus, in this work, the standard LDA (with the Perdew and Wang[28] formula for exchange-correlation potential) is employed in KKR calculations and the energy gaps are expanded to experimental values[29] (see, Table I) to allow for reasonable discussion of transport properties in function of temperature.

B. Electron transport

The Boltzmann transport theory, which can successfully connect atomic level properties of materials with the macroscopic transport coefficients[16,33–35] is used for calculation of thermopower. Within this approach[32] the Seebeck coefficient can be expressed as

$$S = -\frac{1}{eT}\frac{\mathscr{L}^{(1)}}{\mathscr{L}^{(0)}}, \tag{1}$$

where

$$\mathscr{L}^{(\alpha)} = \int d\mathscr{E}\left(-\frac{\partial f}{\partial \mathscr{E}}\right)(\mathscr{E}-\mu_c)^{\alpha}\sigma(\mathscr{E}). \tag{2}$$

$\sigma(\mathscr{E})$ is an energy-dependent conductivity, commonly called the transport function (TF). Chemical potential $\mu_c = \mu_c(T, n_d)$ depends on temperature (T) and doping (n_d), where an extra carrier concentration n_d can be positive ($n-$type doping, e.g. Sb or Bi in Mg_2X) or negative ($p-$type doping, e.g. Ga in some Mg_2(Si-Ge) alloys[11]). In the present work, the rigid band model[36] is used to mimic $n-$ and $p-$type behaviors, which allows to focus on the S-O effect on charge carrier transport in case of electron-like and hole-like doping, respectively.

The transport function, within the relaxation time approximation, has the form of the $\mathbf{k}$-space integral over n electronic bands:[32]

$$\sigma(\mathscr{E}) = e^2\frac{1}{3}\sum_n \int \frac{d\mathbf{k}}{4\pi^3}\tau_n(\mathbf{k})\mathbf{v}_n(\mathbf{k})^2\delta(\mathscr{E}-\mathscr{E}_n(\mathbf{k})), \tag{3}$$

where τ is the electron relaxation time and $\mathbf{v}_n(\mathbf{k}) = \hbar^{-1}\nabla_k\mathscr{E}_n(\mathbf{k})$ denotes the electron velocity. Representing the band structure as isoenergetic surfaces[37] ($\mathscr{E}_n(\mathbf{k}) \to S_n(\mathscr{E})$) and employing the commonly used constant relaxation time approximation ($\tau_n(\mathbf{k}) = \tau_0$) allow to convert TF into the form more convenient for numerical computation:

$$\sigma_\tau(\mathscr{E}) = \tau_0\frac{e^2}{\hbar}\frac{1}{3}\sum_n \int\limits_{S_n(\mathscr{E})} \frac{dS}{4\pi^3}|\mathbf{v}(S_n(\mathscr{E}))|. \tag{4}$$

It is worth mentioning that upon substituting Eq. 4 into Eqs. 3 and 2, τ_0 cancels out so that thermopower is independent of τ_0 in the constant relaxation time approximation.

In a similar way, the density of states (DOS) function can be calculated

$$g(\mathscr{E}) = \sum_n \int\limits_{S_n(\mathscr{E})} \frac{dS}{4\pi^3}\frac{1}{|\nabla_k\mathscr{E}_n(\mathbf{k})|}, \tag{5}$$

and such representation enables to decompose the DOS (and also TF) into contributions from each n-th band.

To facilitate the discussion of the Seebeck coefficient, the effect of the S-O interaction on the effective mass is investigated. Accordingly, we propose a simple and efficient way of calculating the energy dependent effective mass. DOS effective mass is defined for the parabolic band $\mathscr{E}(\mathbf{k}) = \hbar^2\mathbf{k}^2/2m$ through the formula:

$$g(\mathscr{E}) = \frac{m}{\hbar^2\pi^2}\sqrt{\frac{2m\mathscr{E}}{\hbar^2}}. \tag{6}$$

To generalize this concept to any other, non-parabolic case, the effective mass becomes energy (or carrier concentration) dependent $m = m(\mathscr{E})$. The effective mass can be extracted from the DOS formula and combined with its energy derivative

$$m(\mathscr{E}) = m_e m^*(\mathscr{E}) = \hbar^2\sqrt[3]{\pi^4 g(\mathscr{E})g'(\mathscr{E})}, \tag{7}$$

where m_e denotes free electron mass.

TABLE I: The energy band gap in Mg_2X compounds calculated within LDA (E_g^{LDA}) from full-relativistic (FR) or semi-relativistic (SR) KKR methods and compared to experimental values (E_g^{exp})[29]. Experimental lattice constants[6] (a) are also given.

	a (Å)	E_g^{LDA}(eV)		E_g^{exp} (eV)
		SR	FR	
Mg_2Si	6.336	0.32	0.33	0.78
Mg_2Ge	6.385	0.21	0.23	0.72
Mg_2Sn	6.765	-0.17	-0.25	0.35

In this way, the dimensionless DOS effective mass (m^*) can be found at every energy point, at which DOS was calculated. This approach can also be seen as fitting the effective mass with the parabolic band at every $\mathscr{E}$ and **k**-points separately and then averaging over isoenergy surface $S_n(\mathscr{E})$. Practically, the computation of m^* using this scheme requires highly accurate DOS function to avoid problems with numerical noise appearing when differentiating. Here, DOS is calculated with $\Delta\mathscr{E} \sim 9$ meV energy resolution, and $m^*(\mathscr{E})$ resulting from Eq. 7 in final step is smoothed by convolution with the Gauss function with standard deviation $3 \times \Delta\mathscr{E}$. Comparison of the raw and smoothed results is done in Fig. 4.

III. RESULTS

A. Band Structure

Electronic band structures of Mg_2X as calculated from the fully relativistic (FR) and semi-relativistic (SR) KKR methods, are shown in Fig. 1. Generally, electronic structure below the energy gap consists of four occupied bands. The lowest lying and separate band, essentially of $s-$symmetry, is located well below the Fermi energy and other three bands are forming main block of valence states (strongly hybridized $s-$Mg and $p-X$ states), with the bands maxima at Γ point in Brillouin zone (BZ). These three bands are labeled as heavy hole (HH), light hole (LH) and split-off (SO) bands, respectively.

The spin-orbit coupling removes the band degeneracy at Γ point, pushing the SO band down in energy in different way in Mg_2X compounds. The conduction bands have the lowest energy value at the X point in BZ, yielding an indirect band gap in all Mg_2X compounds. It was shown[6,16] that relative position of the two lowest conduction bands mutually change with X atom in Mg_2X, which is clearly seen in the Fig. 1.

TABLE II: The values of spin-orbit splitting at Γ point in Mg_2X compounds.

	Mg_2Si	Mg_2Ge	Mg_2Sn
Calculated (meV)	36	208	525
Measured (meV)	30[a]	200[a]	480[a],600[b]

[a]Ref. 38
[b]Ref. 39

As expected, the importance of relativistic effects gradually increases with increasing atomic number of the X element. In Fig. 1 the difference between SR and FR, as induced by the S-O coupling, can be easily detected for Mg_2Sn and also Mg_2Ge, while it is hardly visible in this energy range for Mg_2Si. The S-O interaction manifests most strongly for the valence bands around the Γ point. It is best seen in Fig. 2 where tentatively three relativistic effects can be observed.

The first effect (as above-mentioned) is removing the degeneracy of electronic states at Γ point by the S-O splitting, Δ_{S-O}, of the $p^{3/2}$ and $p^{1/2}$ orbitals. As a result, the SO band is moved towards lower energy with the Δ_{S-O} values (see Table II) strongly increasing with the atomic number of X atom. Starting from $\Delta_{S-O} = 36$ meV for in Mg_2Si, through $\Delta_{S-O} \simeq 208$ meV in Mg_2Ge, the largest $\Delta_{S-O} \simeq 525$ meV is reached in the heaviest Mg_2Sn compound. Overall, a good agreement between the KKR results and the experimental data derived from infrared spectroscopy measurements is found.

The second modification of the band structure of Mg_2X induced by the S-O interaction, is removing of HH and LH band degeneracy, which appears in some BZ parts (e.g. along Γ-L-X directions) from the semi-relativistic KKR calculations. This splitting is smaller, comparing to the splitting of $p^{3/2}$ and $p^{1/2}$ orbitals at Γ, however at the L point it can also reach considerable values, i.e. 287 meV (X = Sn), 118 meV (X = Ge) and 23 meV (X = Si).

The third and also the most subtle effect, visible actually on an enlarged scale only (Fig. 2), is related to the modification of the bands shapes, which at first glance suggests a decrease of m^* (as discussed below). On the whole, the three aforementioned effects are expected to markedly influence thermopower behaviors in Mg_2X compounds (see Sec.III B).

The magnitude of overall relativistic effects as well as the S-O splitting of the band structure near the Γ point is well illustrated in Fig. 3, where Fermi surfaces (FS) for Mg_2Sn at a hole concentration $p = 10^{21}$ cm^{-3} are plotted. Similar comparison of FR and SR results for $p-$type Mg_2Si and also Mg_2Ge are less pronounced on corresponding FS and they are not presented. We see that the high velocity (red color in the Fig. 3) hole pocket centered at Γ, becomes the SO band pocket and is shifted out the Fermi surface at the hole concentration $p = 10^{21}$ cm^{-3}. Also, the change in the FS curvature can be easily noticed.

The S-O interaction effects, as described above, first of all lower DOS near the valence band edge. This is accompanied by a decrease of the DOS effective mass, which likely reduces the thermopower. The effective mass calculated with use of Eq. 7, is shown in Fig. 4. The reduc-

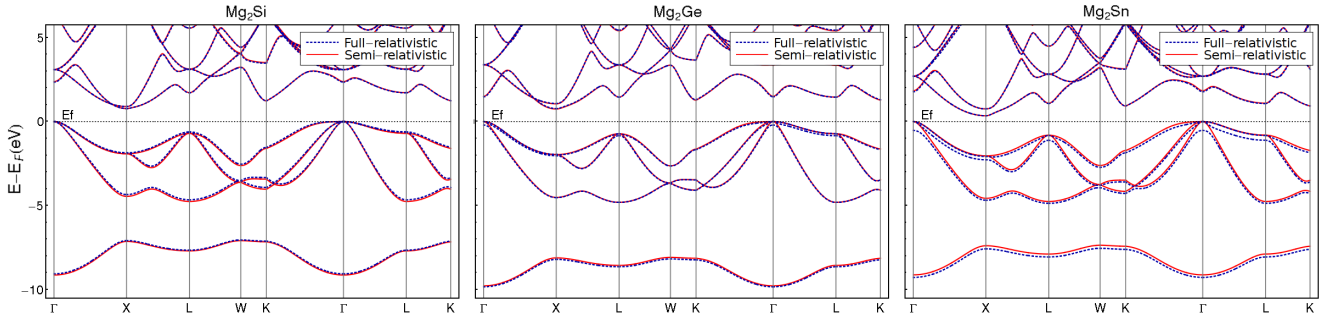


FIG. 1: (Color online) Electron dispersion curves for Mg_2Si (left), Mg_2Ge (middle) and Mg_2Sn (right) as resulted from semi-relativistic and full-relativistic KKR calculations. In each figure, the Fermi level E_F was shifted to top of valence bands (Γ point) and energy gaps were expanded to the experimental values (see text and Table I).

tion of m^* by the S-O interaction is clearly seen for the Mg_2Ge and Mg_2Sn compounds, where it reaches around 50% (dropping from $\sim$ 1.1 to $\sim$ 0.5 m_e in the latter). Such an important reduction can not be explained by the shift of the high velocity SO band, and the change of mass is mainly attributed to modification of the $\mathscr{E}(\mathbf{k})$ slope of the HH and LH bands (see, Fig. 2). The bottom-right panel in Fig. 4 shows the effective mass of $p-$type Mg_2Sn as resulted from the FR and SR calculations, decomposed into all three band contributions. This clearly evidences, that actually the whole contribution to the effective mass comes from the HH band. Bearing in mind that effective mass is a additive quantity due to formula $m^*_{all} = \left(\sum_i {m_i^*}^{3/2}\right)^{2/3}$, the modification of bands curvature by the S-O interaction is the most important effect for the decrease of m^*, more significant than the splitting of bands near Γ. The same can be concluded from Fig 5, where the reduction of total DOS (g) is much larger than the SO band contribution, which is very low due to high velocity ($g \sim 1/v$).

We can also notice an interesting topological feature of the dispersion relations in the FR case: the LH band

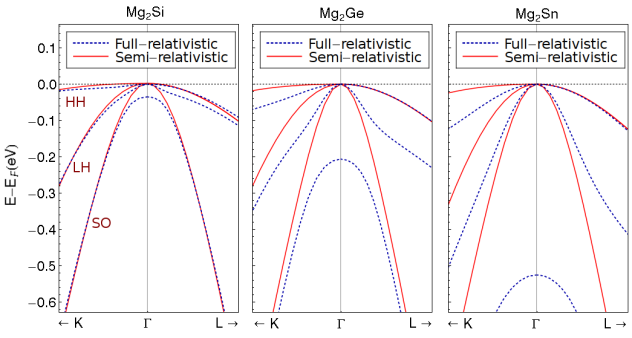


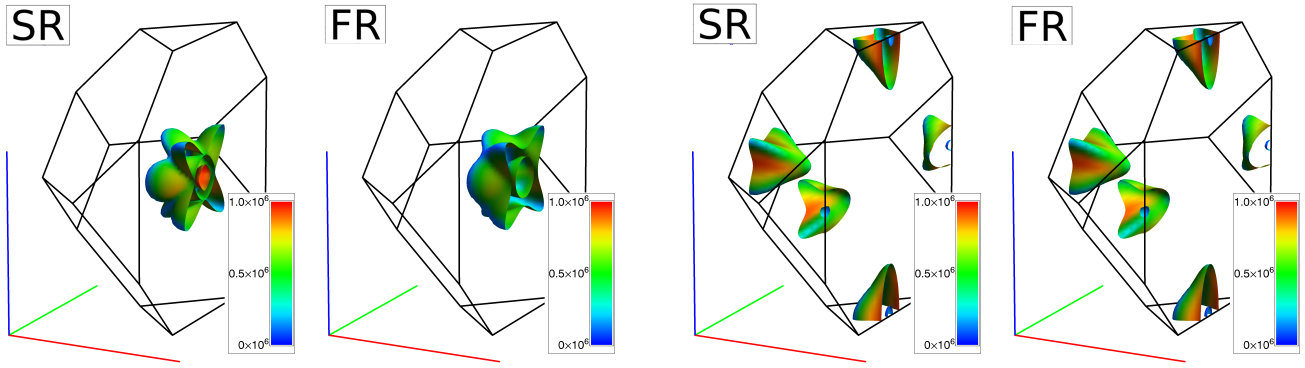
FIG. 2: (Color online) Zoom of the three valence bands of Mg_2X along the K-Γ-L direction as computed from SR and FR calculations. The spin-orbit interaction removes the degeneracy of bands at Γ, and the largest splitting is observed for the Sn case. Subtle topological effects are evidently detected for the LH band (see text).

is convex along the Γ-L direction, close to the valence band edge. In the SR case, the flexion point, at which the $\mathscr{E}(\mathbf{k})$ function changes from convex to concave, lies at much deeper energy. The S-O interaction moves this flexion point in the energy (and carrier concentration) range important for the TE properties. This convex $\mathscr{E}(\mathbf{k})$ function locally leads to the positive effective mass, i.e. there is an electron-like, compensating contribution to the overall hole-like electronic properties. This FS feature reduces the LH band effective mass, being another source of lowering of m^*. This behaviour resembles the case of PbTe-PbS alloy[30], where similar topological effect of the local convex shape of the valence band leads to the negative Seebeck coefficient at low temperatures.

In Mg_2Ge compound the HH band modifications as well as energy splitting of the bands is smaller than in Mg_2Sn, and, as a consequence, the effective mass reduction is limited to the narrow energy range near the valence band edge.

In Mg_2Si the effect is opposite to the previously discussed cases. Fully relativistic treatment yields c.a. 10% rise of the value of effective mass, due to the $\mathscr{E}(\mathbf{k})$ slope change, except for the range just below the valence band edge, where the SO band moves out and local convex $\mathscr{E}(\mathbf{k})$ function shows up.

The analysis of the effective mass suggests how the spin-orbit interaction will modify the thermopower of the system, since $S \propto m^*$. For the Mg_2Sn we may expect strong reduction of the $p-$type thermopower, for the Mg_2Ge the reduction of thermopower is expected only at low concentration in $p-$type materials, and the increase of the Seebeck coefficient for Mg_2Si can be predicted. Lowering of thermopower in Mg_2Sn system can also be deduced from transport function in Fig 5, where its strong lowering in $p-$type doping is seen in FR calculation. It is also worth noting that the SO band has negligible influence on total TF (and therefore thermopower), which is not so evident accounting for the fact that TF is a function sensitive to electron's velocity ($\sigma \sim v^2$) and the SO band has the highest value of v up to 1.0×10^6 ms^{-1} (see next paragraph for detailed calculation of thermopower).



(a) p-type Mg_2Sn (b) n-type Mg_2Sn

FIG. 3: (Color online) Fermi surfaces of $p-$type (a) and $n-$type (b) Mg_2Sn plotted for carrier concentration 10^{21} cm^{-3}. In both cases semi-relativistic (SR) and fully relativistic (FR) results are compared. Electron velocities (in m/s) are represented by colors.

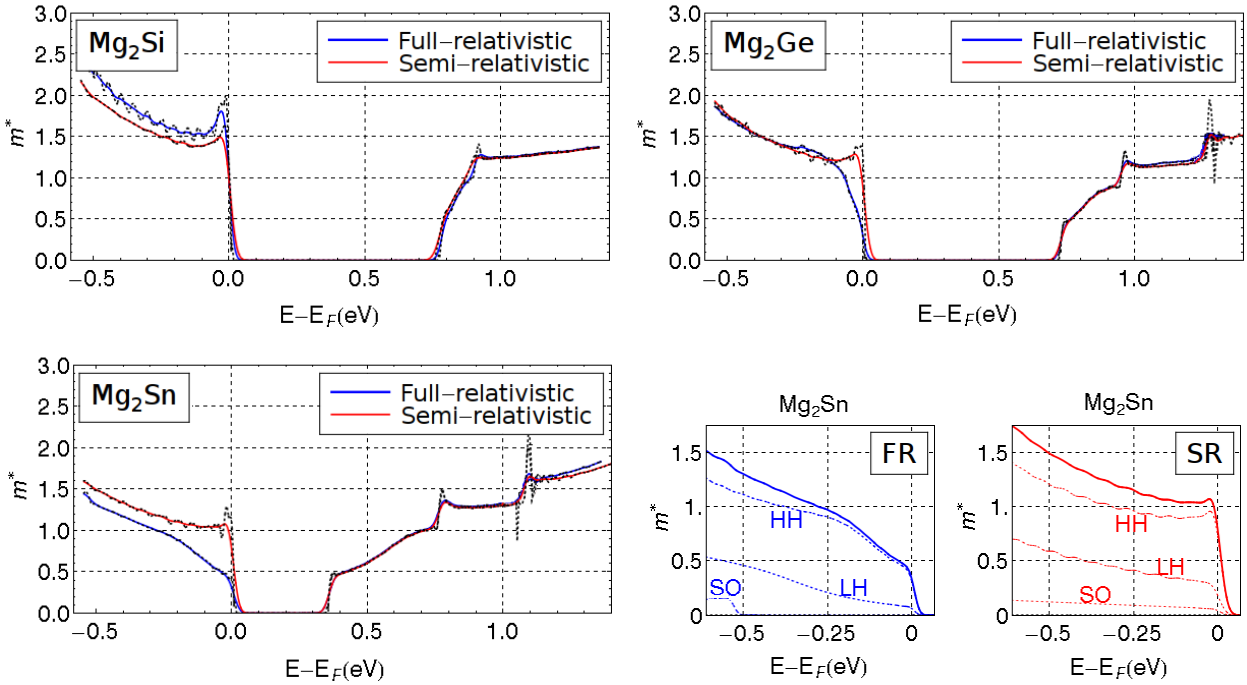


FIG. 4: (Color online) DOS effective mass of carriers near the band gap in Mg_2X compounds. Bottom-right panel shows the effective hole mass corresponding to the heavy-hole (HH) light-hole (LH) and split-off (SO) bands for full-relativistic (FR) and semi-relativistic (SR) results. The spin-orbit interactions mostly affect mass of heavy holes.

As far as the conduction bands are concerned, no significant difference between FR and SR calculations are observed, even in the case of Mg_2Sn. The Fermi surfaces and also the effective masses do not show any difference for $n-$type doping as large as $n = 10^{21}$ cm^{-3}(see Figs. 3b and 4).

B. Thermopower

Thermopower of Mg_2X compounds, calculated in the constant relaxation time approximation and using Eqs. 1-4, are shown in a wide range of carrier concentration for both $n-$ and $p-$type in Fig. 6. In addition, for the carrier concentrations $n = p = 10^{20}$ cm^{-3} and at three selected temperatures (70 K, 300 K and 900 K) the Seebeck coefficient values are gathered in Table III. The results

TABLE III: Seebeck coefficient (FR and SR results) at $n = p = 10^{20}\text{cm}^{-3}$ for different temperatures in Mg_2X compounds.

		Mg_2Si			Mg_2Ge			Mg_2Sn		
		70 K	300 K	900 K	70 K	300 K	900 K	70 K	300 K	900 K
n-type	S_{FullRell} (μV/K)	-33	-139	-291	-27	-113	-273	-20	-84	-214
	S_{SemiRell} (μV/K)	-34	-141	-290	-27	-112	-269	-19	-82	-207
	$S_{\text{FR}}/S_{\text{SR}}$ (-)	98%	99%	100%	100%	101%	101%	103%	102%	104%
p-type	S_{FullRell} (μV/K)	77	208	329	41	154	305	22	94	224
	S_{SemiRell} (μV/K)	65	191	314	62	189	310	47	156	263
	$S_{\text{FR}}/S_{\text{SR}}$ (-)	118%	109%	105%	67%	83%	98%	48%	60%	85%

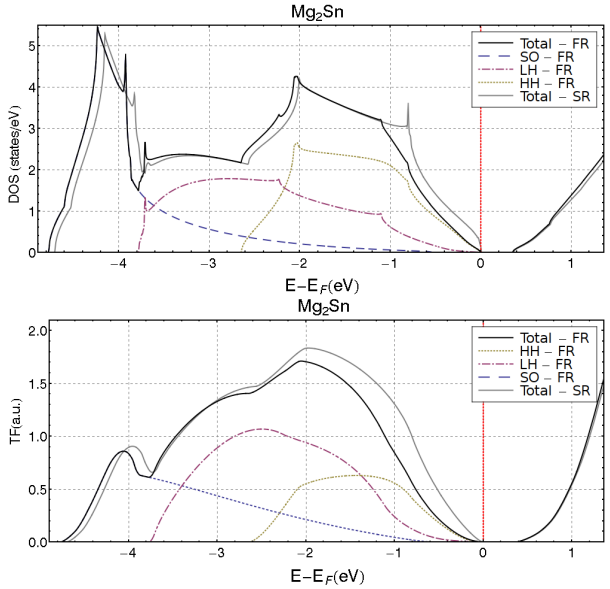


FIG. 5: (Color online) Density of states (DOS) and transport function (TF) of Mg_2Sn with decomposition on bands calculated with full-relativistic (FR) method. For comparison DOS and TF are also shown for semi-relativistic (SR) case.

of the Boltzmann transport and KKR calculations are consistent with intuitive predictions based on the aforementioned analysis of the band splitting and effective mass changes. First of all, for the three Mg_2X compounds there is no significant difference between thermopower from FR and SR calculations in the $n-$type materials for high concentration and low temperature. The reason is simply the negligible differences between conduction bands induced by the S-O interaction. On the other hand, the difference between FR and SR appearing for lower carrier concentration and higher temperature comes from the bipolar effect, which accounts for contribution from valence bands, that are apparently different from the FR and SR results. The bipolar reduction of the absolute value of $n-$type S is highest for Mg_2Sn, where the band gap is the smallest. In fully relativistic KKR calculations Seebeck coefficient is less reduced, because of the lower effective mass of holes.

For hole-like thermopower, the splitting of the bands accompanied by the reduction of the effective mass significantly decrease the Seebeck coefficient in Mg_2Ge and Mg_2Sn for $p < 10^{21}$ cm^{-3} in the low and mid-temperature range (see also Tab. III). For Mg_2Sn, the S-O effect can lower thermopower even twice, showing that it is crucial for the discussion of the TE properties of $p-$type Mg_2X systems. At high temperature, due to the temperature blurring of DOS (convoluted with Fermi-Dirac function), the main contribution to thermopower comes from the lower-lying parts of dispersion curves, where computed band curvature from FR and SR approaches, are similar. Also, at high temperature the importance of the SO band splitting diminishes, which effectively lowers the difference between SR and FR computations. Similar trend is apparently observed when the carrier concentration increases and the Fermi level moves deeper into the valence bands and almost no difference between SR and FR results is observed for $p > 10^{21}$ cm^{-3}.

Interestingly, FR KKR calculations show that in $p-$type Mg_2Si both m^* and S values are in principle higher than the values from the SR computations. The slightly reduced S is seen only in very low concentration and temperature, where the small area of FS near Γ point are taken into consideration in electron transport. In this case, i.e. $p < 1\times10^{19}$, the band curvature modification as well as the S-O splitting, seen in the Fig. 2, leads to the decrease of m^*, and therefore to small decrease of S (see Fig 6 at $T = 70$ K and small hole concentration p). For $p > 1 \times 10^{19}$, these effects are no longer important. At higher temperature the S-O splitting is too small and additionally smeared by temperature, i.e. $\Delta_{S-O} = 30$ meV $= k_BT$ for $T \sim 350$ K, that it does not alter results from transport function integration (Eq. 1).

IV. SUMMARY

The results of the electronic band structure calculations with the use of fully relativistic (FR) vs. semi-

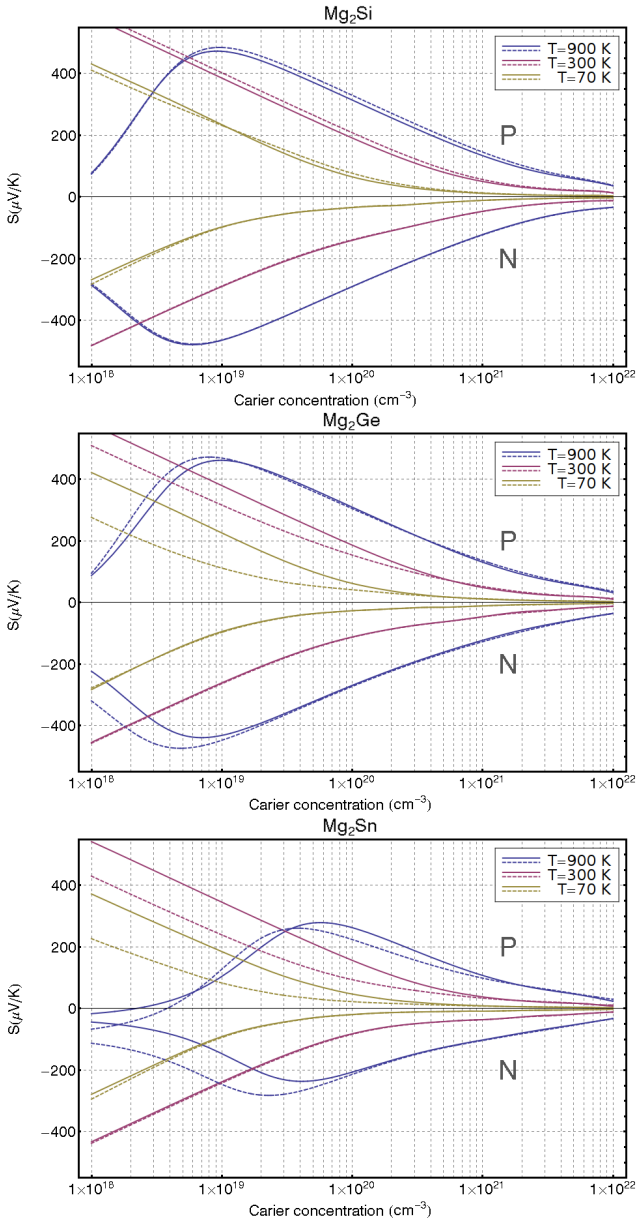


FIG. 6: (Color online) Thermopower of Mg_2Si (top), Mg_2Ge (middle) and Mg_2Sn (bottom) as a function of carrier concentration for selected temperatures. Solid lines show semi-relativistic and dashed line full-relativistic results, respectively.

relativistic (SR) full potential KKR method for the Mg_2X (X = Si, Ge and Sn) compounds were reported. It was found that the S-O interaction splits the valence band structure, with the S-O splitting at Γ point, namely 36 meV, 208 meV and 525 meV, well corresponding to experimental data[38,39] 30 meV, 200 meV and 480 meV (or 600 meV) in Mg_2Si, Mg_2Ge and Mg_2Sn, respectively. The S-O splitting itself, as well as modification in dispersion relation (even more important) of top valence bands, i.e. heavy and light hole bands, significantly decreased the effective mass and the Seebeck coefficient. In Mg_2Ge and Mg_2Sn, the analysis of the energy dependent DOS effective mass shows that the S-O interaction lowers m^* of holes, and the effect is larger near the valence band edge and for the heaviest compound. In general, this leads to the reduction of the $p-$type thermopower, mostly at lower concentration and low or medium range of temperature. The thermopower decrease becomes more serious with increasing atomic number of X element, reaching the magnitude of 50% in Mg_2Sn. On the whole, our KKR calculations combined with Boltzmann transport approach clearly show that the relativistic effects are detrimental for thermoelectric performance in $p-$doped Mg_2Ge and Mg_2Sn. In Mg_2Si, the S-O interaction slightly increases the effective hole mass, except for the low carrier concentration range. This behavior leads to the small increase of thermopower (up to 10%) for $p > 10^{19}$ cm^{-3}.

In turn, the S-O coupling effect on the conduction bands is negligible in all Mg_2X compounds. Surprisingly, the $n-$type thermopower at lower carrier concentrations benefits from the degradation of the $p-$type S due to the reduction of the bipolar effect, which is well seen in Mg_2Ge and Mg_2Sn compounds.

In summary, the full relativistic KKR results revealed that the spin-orbit interaction is significant factor decreasing the thermoelectric performance of $p-$type Mg_2X (especially Mg_2Sn). They also enlightened the reason why in Mg_2(Si-Ge-Sn) system the measured zT in $p-$doped samples was much lower ($zT < 0.4$)[11] than the values gained in $n-$doped materials ($zT \sim 1.4$)[10,40].

Acknowledgments

This work was supported by the Polish National Science Center (NCN) under the grants DEC-2011/02/A/ST3/00124 and UMO-2011/03/N/ST3/02644, Thermomag project (FP7-NMP4-SL-2011-263207) co-funded by the European Space Agency and by individual partner organizations as well as by the Polish Ministry of Science and Higher Education.

* kamil.kutorasinski@fis.agh.edu.pl

[1] U. Winkler, *Helv. Phys. Acta* **28** 633 (1955)
[2] R. G. Morris, R. D. Riedin, and G. C. Danielson, *Phys. Rev.* **109** 1909 (1958)
[3] E. N. Nikitin, V. G. Basanov, and V. I. Tarasov, *Sov. Phys. Solid State* **3** 2648 (1961)
[4] R. J. Labotz, D. R. Mason, D. F. O'Kane, *J. Electrochem. Soc.* **110** 127 (1963)

[5] Y. Noda, H. Kon, Y. Furukawa, I. A. Nishina, K. Matsumoto, *Mater. Trans. JIM* **33** 851 (1992)

[6] V. K. Zaitsev, M. J. Fedorov, E. A. Gurieva, I. S. Eremin, P. P. Konstantinov, A. Y. Samunin and M. V. Vedernikov, *Phys. Rev. B* **74**, 045207 (2006)

[7] J. I. Tani, and H. Kido *Physica B* **364** 218 (2005)

[8] A. Y. Samunin, V. K. Zaitsev, P. P. Konstantinov, M. J. Fedorov, G. N. Isachenko, A. T. Burkov, S. V. Novikov, and E. A. Gurieva *J. Electron. Mater.* **42** 1676 (2013)

[9] J. Bourgeois, J. Tobola, B. Wiendlocha, L. Chaput, P. Zwolenski, D. Berthebaud, F. Gascoin, Q. Recour and H. Scherrer, *Func. Mater. Lett.* **6** 1340005 (2013)

[10] A. U. Khan, N. Vlachos and Th. Kyratsi *Scripta Mater.* **69** 8 606, (2013)

[11] H. Ihou-Mouko, C. Mercier, J. Tobola, G. Pont, H. Scherrer, *J. Alloys Compd. 509* 6503 (2011)

[12] K. Mars, H. Ihou-Mouko, G. Pont, J. Tobola, and H. Scherrer, *J. Electron. Mater.* **38** 1360 (2009)

[13] W. Liu, X. Tan, K. Yin, H. Liu, X. Tang, J. Shi, Q. Zhang, and C. Uher, *Phys. Rev. Lett.* **108** 166601 (2012)

[14] J. J. Pulikkotil, D. J. Singh, S. Auluck, M. Saravanan, D. K. Misra, A. Dhar, and R. C. Budhani *Phys. Rev. B* **86**, 155204 (2012)

[15] X. J. Tan, W. Liu, H. J. Liu, J. Shi, X. F. Tang, and C. Uher *Phys. Rev. B* **85** 205212 (2012)

[16] K. Kutorasinski, J. Tobola, and S. Kaprzyk, *Phys. Rev. B* **87**, 195205 (2013)

[17] J. Tobola, S. Kaprzyk, and H. Scherrer *J. Electron. Mater.*, **39**, 2064 (2010)

[18] P. Zwolenski, J. Tobola, and S. Kaprzyk, *J. Electron. Mater.* **40**, 889 (2011)

[19] H. Kohn and N. Rostoker *Phys. Rev.* **94** 1111 (1954)

[20] W. H. Butler *Phys. Rev. B* **14** 468 (1976)

[21] S. Kaprzyk and A. Bansil *Phys. Rev. B* **26**, 367 (1982)

[22] S. Kaprzyk and A. Bansil *Phys. Rev. B* **42**, 7358 (1990)

[23] A. Bansil, S. Kaprzyk, P. E. Mijnarends and J. Tobola, *Phys. Rev. B* **60**, 13396 (1999).

[24] T. Stopa, S. Kaprzyk, J. Tobola *J. Phys.: Condens. Matter* **16**, 4921 (2004)

[25] D.D. Koelling and B.N. Harmon *J. Phys.C: Solid State Phys* **10** 3107 (1977)

[26] H. Ebert, H. Freyer and M. Deng, *Phys. Rev. B* **56**, 9454 (1977)

[27] T. Stopa, J. Tobola, S. Kaprzyk, E. K. Hlil. and D. Fruchart *J. Phys.: Condens. Matter* **19** 6379 (2006)

[28] J. P. Perdew and Y. Wang *Phys. Rev. B* **45**, 13244 (1992)

[29] V.K. Zaitsev, M.I. Fedorov, I.S. Eremin, and E.A. Gurieva in *Thermoelectrics Handbook: Macro to Nano Edited by* D.M.Rowe, Taylor and Francis (2006)

[30] C. M. Jaworski, M. D. Nielsen, H. Wang, S. N. Girard, W. Cai, W. D. Porter, M. G. Kanatzidis, and J. P. Heremans Phys. Rev. B **87**, 045203 (2013).

[31] F. Tran and P. Blaha *Phys. Rev. Lett.* **102**, 226401 (2009)

[32] N.W. Ashcroft N.D. Mermin *Solid State Physics*, 1976

[33] T. Thonhauser, T. J. Scheidemantel, J. O. Sofo, J. V. Badding, and G. D. Mahan, Phys. Rev. B **68**, 085201 (2003).

[34] G. K. H. Madsen, K. Schwarz, P. Blaha, and D. J. Singh, *Phys. Rev. B* **68**, 125212 (2003)

[35] L. Chaput, P. Pecheur, J. Tobola, and H. Scherrer, *Phys. Rev. B* **72**, 085126 (2005)

[36] E. A. Stern *Phys. Rev.* **157** 544 (1967)

[37] W. E. Lorensen, *Computer Graphics*, Vol. **21**, Nr. 4, July 1987

[38] F. Vazquez, A. R. Forman, and M. Cardonna *Phys. Rev.*, vol. 176, p. 905, 1968

[39] L. A. Lott and D. W. Lynch, Phys. Rev. 141, 681 (1965) [CAS].

[40] W. Liu,Q. Zhang,K. Yin, et al *Journal Of Solid State Chemistry* **203**, 333-339, (2013)